# CHAPTER VIII

# THE DEVELOPMENT OF METHANOL FUEL PROCESSOR OVER GOLD-BASED CATALYSTS: EFFECTS OF SINGLE AND DOUBLE STAGES FOR PREFERENTIAL CO OXIDATION*

## 8.1 Abstract

The methanol fuel processor (MFP), consisting of steam reformer (SRM) and preferential CO oxidation (PROX), was optimized for minimizing carbon monoxide (CO) concentration under Au-based catalysts prepared by deposition-precipitation (DP)—SRM; Au–Cu/$Ce_{0.75}Zr_{0.25}O_2$ and PROX; Au/$CeO_2$. Many effective parameters were studied for both single- and double-stage PROX reactors such as $O_2$/CO feed ratio, amount of use catalyst, $O_2$ and weight split ratios, and reaction temperature under the fixed conditions of SRM. The optimum conditions of the single-stage revealed that the uses of 500 mg catalyst and unity $O_2$/CO ratio obtained the low CO and $O_2$ conversions at ~60 % and ~78 %, respectively, in the whole range of 90–150 °C. Within the same previous conditions, the superior improvements of PROX activity at—98 % CO conversion, full $O_2$ conversion, and CO concentration at the output stream of 300–700 ppm—were achieved after introducing the double-stage PROX with the uses of $O_2$ split ratio = 50:50, catalyst weight split ratio = 0.35:0.15, and the first-stage temperature ($T_{1st\ stage}$) of 110 °C. The variation of $T_{1st\ stage}$ significantly affected the double-stage PROX performance, when compared to other parameters. The use of double-stage PROX was necessary to enhance the $H_2$ purity in the MFP process. The contamination of the $CO_2$ and $H_2O$ in the reformate did not degrade much on the stability of Au/$CeO_2$ catalyst.

**Keywords**: Methanol Fuel Processor; Hydrogen; CO conversion; Carbon monoxide; Au catalyst; Reformate

---

*In preparation.

## 8.2 Introduction

Nowadays, the use of proton exchange membrane fuel cell (PEMFC) is attractive to many mobile engines due to its green technology and high efficiency to generate an electrical power. Only requirement of PEMFC is the high purity of hydrogen ($H_2$) feeding stream that contains carbon monoxide (CO) not higher than 10 ppm because CO can extremely poisoned and deteriorated the Pt electrode inside the fuel cell, related with its performance [1–4]. Even though the main route to produce rich-$H_2$ gas was widely known as the steam reforming of liquid fuel (hydrocarbon and alcohol), the amount of CO by-product gas was still not acceptable for applying in PEMFC [5–7]. In some cases, the CO reduction unit was coupled with the reforming unit to specifically minimize the CO amount such as PROX and water-gas shifted (WGS) processes, where this combination process was also named as "Fuel Processor" [8–10]. It was noteworthy that the selection of the fuel used in the reformer was effective to the CO amount in the product stream (reformate) before sending to the CO reduction unit. Among of the fuel reactants, methanol ($CH_3OH$) fuel seems to be promising due to its lower operating temperature of 200–400 °C that was beneficial for saving energy during producing high $H_2$ purity gas. The developments of methanol fuel processor (MFP) have been variously studied in the reformer unit (methanol decomposition (DM) [11], steam reforming (SRM) [12,13], partial oxidation (POM) [14], and oxidative steam reforming (OSRM) [14]), a type and number of CO reduction stages, the operating temperature, and the selection of use catalyst [8,15,16].

Taking into account the selection of catalyst, noble metal catalyst, especially for gold (Au) catalyst, was received much attention in recently due to its high activity in both $H_2$ production and CO oxidation at low operating temperature. However, the improvement of Au-based catalysts strongly depends on the metal oxide support selection [17], the co-additional precious metal with Au to form bimetallic catalyst [18,19], gas pretreatment [20], calcination temperature [4,5], and so on. For now, we synthesized the superior Au–Cu/$CeO_2$–$ZrO_2$ bimetallic catalyst which consisted of two active sites from (i) Au–Cu alloy at the metal site and (ii) $Ce_{1-x}Zr_xO_2$ solid solution at the support site, that were responsible for the full $CH_3OH$ conversion

within the ultra-low CO selectivity (~10 000–13 000 ppm) in the SRM, including high thermal stability at 300 °C without sintering deactivation [20,21]. To fulfill our work in the MFP development, the reformate was then sent to the PROX process before being applied in the PEMFC. Focusing in on the PROX process, the 1 wt% $Au/CeO_2$ catalyst was chosen for using in this case since it normally has the good activity by itself [22]. In the PROX optimization, not only did the use of Au catalyst, but a number of stages (or reactors) and the $O_2$ feeding amount also affected the PROX performance [23]. In 2008, Nakham and co-workers compared between single- and double-stage PROX, and found that the double-stage extremely enhanced the CO conversion without affecting the $H_2$ amount in the simulated reformate via $H_2$ oxidation [23]. Consequently, the main objective of this experiment was to optimize the PROX unit in the MFP to obtain high $H_2$ purity at low temperature under the uses of Au-based catalysts ($Au–Cu/CeO_2–ZrO_2$ in SRM and $Au/CeO_2$ in PROX). The studied parameters—$O_2$/CO feed molar ratio, calcination temperature, reaction temperature, $O_2$ split ratio, and catalyst weight split ratio—were optimized, while keeping the conditions of SRM constantly as previously [20].

## 8.3 Experimental

### 8.3.1 Catalyst preparation

The catalyst preparation was divided into two sections; bimetallic catalyst ($Au–Cu/CeO_2–ZrO_2$) and monometallic catalyst ($Au/CeO_2$). All of them were prepared by deposition-precipitation (DP) method.

#### *8.3.1.1 Monometallic preparation*

For the $CeO_2$ support, the 0.1 M of salt solutions of cerium (III) nitrate hexahydrate [$Ce(NO_3)_3.6H_2O$; Aldrich] and $Na_2CO_3$ (Riedel-de Haen) were mixed under vigorous stirring conditions at 80 °C and pH 8. Afterwards, the precipitate was washed with warm deionized water to eliminate residual ions. The deionized precipitate was dried at 110 °C and calcined in air at 400 °C for 4 h in order to obtain the $CeO_2$ support [4,5].

In order to obtain the 1 wt% $Au/CeO_2$, the prepared $CeO_2$ support was then deposited by an aqueous solution of $HAuCl_4.3H_2O$ (Alfa AESAR) under vigorous stirring conditions at 80 °C and pH 8, adjusted by the addition of $Na_2CO_3$. The resulting solution was stirred for 1 h, then washed, dried, and calcined in air at 300 and 400 °C for 4 h.

*8.3.1.2 Bimetallic preparation*

The $CeO_2$–$ZrO_2$ mixed oxide support was prepared by the co-precipitation (CP) method, as reported in elsewhere [20,21]. Appropriate amounts of 0.1 M aqueous solutions—$Ce(NO_3)_3.6H_2O$, zirconium (IV) oxide chloride octahydrate [$ZrOCl_2.8H_2O$; Merck], and $Na_2CO_3$—were mixed under vigorous stirring conditions at 80 °C and pH 8 to obtain the $Ce_{0.75}Zr_{0.25}O_2$ solid solution. Afterwards, the precipitate was washed with warm deionized water to eliminate residual ions. The deionized precipitate was dried at 110 °C and calcined in air at 400 °C for 4 h in order to obtain the support.

For the Au–Cu co-deposition (3.5 wt% Au–3.5 wt% Cu or Au/Cu atomic ratio of 1/3), two metal aqueous solutions—copper (II) nitrate trihydrate [$Cu(NO_3)_2.3H_2O$; MERCK] and $HAuCl_4.3H_2O$—were mixed under vigorous stirring conditions of 80 °C and pH 7. The resulting solution was then washed, dried, and calcined in air at 300 °C for 4 h [20,21].

8.3.2 Catalyst characterization

An X-Ray Fluorescence Spectrometer, XRF (AXIOS PW4400), was used to determine the actual surface (Au, Cu, Ce, and Zr) composition.

Powder XRD measurements were carried out on a JEOL X-Ray diffractometer system (JDX-3530) with a $CuK_\alpha$ (1.5406 Å) X-ray source operating at 40 kV and 30 mA.

The sizes of the Au and Au–Cu alloy particles deposited on the supports were directly observed by a transmission electron microscope, TEM (JEOL, JEM 2010), at an accelerating voltage of 200 kV in bright field mode. Before being transferred into the TEM chamber, the samples were dispersed in ethanol and then

dropped onto a copper grid. The volume-area average Au particle size diameter ($d_{TEM}$) was calculated from the following formula: $d_{TEM} = \Sigma(n_i d_i^3)/(n_i d_i^2)$, where $n_i$ is the number of Au particles of diameter $d_i$.

The Fourier transform infrared spectra (FTIR) of the spent catalysts were recorded using a Thermo Nicolet Nexus 670 FTIR spectrometer in absorbance and transmittance mode at 32 scans with a resolution of 4 $cm^{-1}$. The spectra in the frequency range of 4000 to 400 $cm^{-1}$ were obtained by using a deuterated triglycerinesulfate detector with a specific detectivity of $1 \times 10^9$ cm $Hz^{1/2}$ $w^{-1}$.

Temperature-programmed reduction (TPR) of the catalysts was carried out in a conventional TPR reactor with a 30 ml/min of 10% $H_2$ in argon with a conventional TPR reactor equipped with a thermal conductivity detector. The reduction temperature was raised from 30 to 850 °C at a ramp rate of 10 °C $min^{-1}$.

### 8.3.3 Catalytic activity measurements

#### *8.3.3.1 SRM*

The overall process flow diagram of the MFP has been showed in the Fig. 8.1. Firstly, the SRM reaction was carried out in a fixed-bed reactor containing 100 mg of Au–Cu/$CeO_2$–$ZrO_2$ catalyst under atmospheric pressure at 300 °C. The molar ratio of distilled water to methanol was mixed at 2/1 and injected continuously by a syringe pump at a rate of 1.5 mL $h^{-1}$ to a vaporizer, which was mixed with He carrier gas before entering the catalytic reactor. The gas hourly space velocity (GHSV) was kept at 21 000 mL g-$cat^{-1}$ $h^{-1}$. The product gases (e.g. $H_2$, CO, $CO_2$, and $CH_4$) from the reactor were analyzed by auto-sampling in an on-line gas chromatograph, Agilent 6890N, with a packed carbosphere (80/100 mesh) column (10 ft x 1/8 inch), and a thermal conductivity detector (TCD). The selectivity of each product gas was defined by the mole percentage in the product stream, and the free-methane products' selectivity of 81 % $H_2$, 1.3 % CO, and 17.7 % $CO_2$ was evaluated in the reformate before sending to the PROX unit.

#### *8.3.3.2 PROX*

The reformate stream from the SRM unit was injected into the PROX reactor with the average total flow rate of 33 mL $min^{-1}$, and the oxygen

gas was fed into the PROX reactor with different $O_2$/CO molar ratios under the use of 100 mg of Au/$CeO_2$ catalysts calcined at 300 and 400 °C, which were packed in the single-stage PROX as the fixed-bed reactor. Afterwards, the amount of catalyst was varied from 100 to 600 mg during the operating temperature range of 90–150 °C. Based on the same optimum conditions as the first-stage PROX, the variations of $O_2$ split ratio, weight split ratios, and reaction temperature of each reactor must be optimized in the double-stage PROX. The GHSV values of both single-stage and double-stage reactors were summarized in Table 8.1. Since the total amount of oxygen gas fed into the PROX unit was very low, this did not interrupt the change in GHSV as much as the variation of catalyst amount. The outlet products from the PROX reactor were directly analyzed by the same on-line gas chromatograph. The CO and $O_2$ conversions were calculated from the moles of CO and $O_2$ consumptions, respectively. The CO concentration was observed at the output stream of the MFP in ppm unit.

**Table 8.1** Summary of the conditions of single- and double-stage PROX reactors

| Type of reactor | $O_2$/CO ratio | $O_2$ split ratio | | Amount of catalyst (mg) | | GHSV (mL g-cat$^{-1}$ h$^{-1}$) | | W/F (g-cat*min mL$^{-1}$) | |
|---|---|---|---|---|---|---|---|---|---|
| | | 1$^{st}$ stage | 2$^{nd}$ stage | 1$^{st}$ stage | 2$^{nd}$ stage | 1$^{st}$ stage | 2$^{nd}$ stage | 1$^{st}$ stage | 2$^{nd}$ stage |
| Single-stage PROX | 0.5 | - | - | 100 | - | 19,800 | - | 0.003 | - |
| | 1.0 | - | - | 100 | - | 19,800 | - | 0.003 | - |
| | 1.0 | - | - | 300 | - | 6,600 | - | 0.009 | - |
| | 1.0 | - | - | 500 | - | 3,960 | - | 0.016 | - |
| | 1.0 | - | - | 600 | - | 3,300 | - | 0.018 | - |
| Double-stage PROX | 1.0 | 60 | 40 | 250 | 250 | 7,920 | 7,920 | 0.008 | 0.008 |
| | 1.0 | 50 | 50 | 250 | 250 | 7,920 | 7,920 | 0.008 | 0.008 |
| | 1.0 | 40 | 60 | 250 | 250 | 7,920 | 7,920 | 0.008 | 0.008 |
| | 1.0 | 50 | 50 | 350 | 150 | 5,657 | 13,200 | 0.011 | 0.005 |
| | 1.0 | 50 | 50 | 150 | 350 | 13,200 | 5,657 | 0.005 | 0.011 |

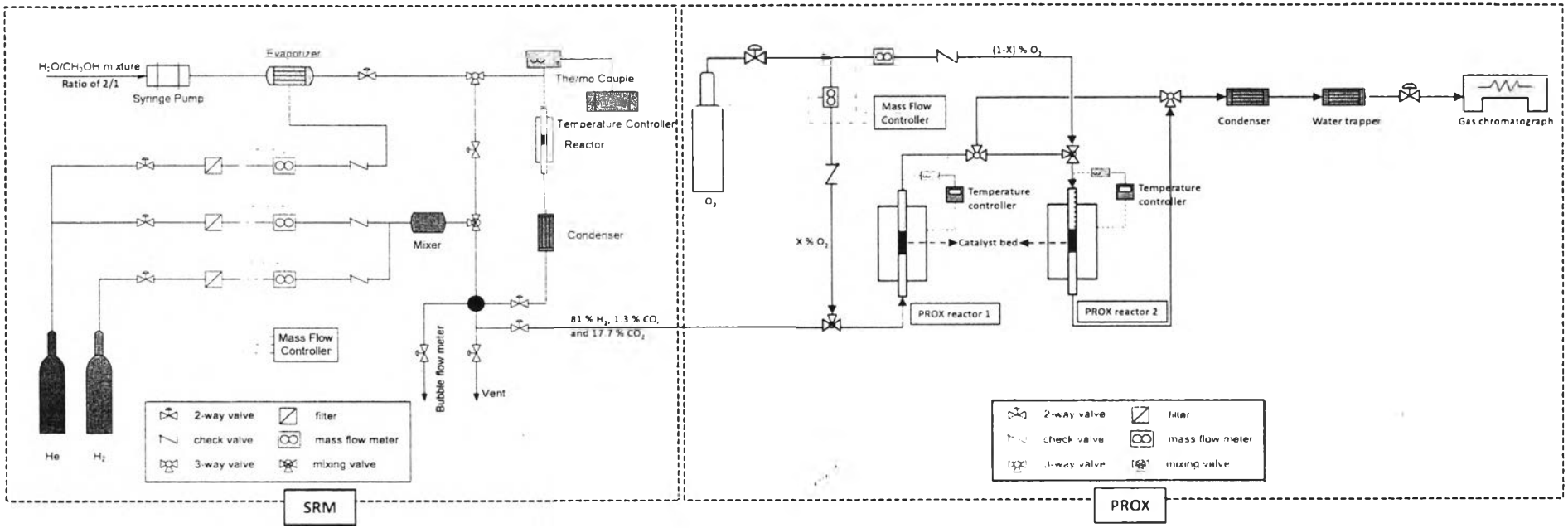


**Figure 8.1** Process flow diagram of the methanol fuel processor (MFP).

## 8.4 Results and discussion

### 8.4.1 Catalyst characterization

According to the Table 8.2, all chemical compositions of DP catalysts were closely to the nominal values, which confirmed the high accuracy of using DP technique. When focusing on the mean ceria crystallite size calculated by the Scherrer equation, those of all fresh and spent samples were around 7.68–8.83 nm, suggesting the slight difference in crystal growth even exposure to the reaction. The XRD patterns of the $Au/CeO_2$ catalysts (Fig. 8.2A) presented many $CeO_2$ diffractions at 2θ of 28.5, 33.08, 47.47, 56.33, 59.08, 69.40, 76.69, and 79.07°, corresponding to $CeO_2$ planes (111), (200), (220), (311), (222), (400), (331), and (420), respectively [24,25]. The increase of $CeO_2$ intensities at the calcination temperature of 400 °C was related with the crystallinity improvement. Meanwhile, the Au diffraction was not detectable in the $Au/CeO_2$, probably due to the highly dispersed Au nanoparticles. For the $Au–Cu/Ce_{0.75}Zr_{0.25}O_2$ catalyst (Fig. 8.2B), the slight shifting to higher 2Θ degree of ceria diffractions, represented the $Zr^{4+}$ incorporation inside the $Ce^{4+}$ lattice to cause the shrinking structure to form solid solution which was confirmed by the reduction of ceria lattice constant from 0.544 nm (pure $CeO_2$) to 0.540 nm ($Ce_{0.75}Zr_{0.25}O_2$), calculated by Bragg's equation [22,26,27]. The appearance of Au (111) diffraction was observed, and it shifted from 38.34° (monometallic Au [20]) to 38.17° in the zoom-in diffraction, as the consequences of adding Cu to form Au–Cu alloy particle. This also resulted in the growth of Au crystallite size in bimetallic catalyst to 13.19 nm, where the highly dispersed CuO particles possibly acted as the shell around the Au core to form larger size [20,21]. Another measurement of $Au_xCu_{1-x}$ alloy formation was the gold lattice constant of 0.4053 nm that was between the pure gold (0.4079 nm) and pure copper (0.3615 nm) [20,28]. The TEM images (Fig. 8.3) showed the highly dispersed Au nanoparticles in the $Au/CeO_2$ with 2.86 nm particle size, while the homogeneous Au–Cu alloy particle sizes at ~38 nm in the bimetallic catalyst was in accordance with the XRD results.

**Table 8.2** Chemical composition and physical properties of the $Au/CeO_2$ and $Au–Cu/CeO_2–ZrO_2$ catalysts

| Catalyst | Total loading | Calcination temperature | Au* | Cu* | Ce* | Zr* | Crystallite size (nm) | |
|---|---|---|---|---|---|---|---|---|
| | (wt%) | (°C) | (wt%) | (wt%) | (wt%) | (wt%) | $CeO_2$[a] | Au[b] |
| $Au–Cu/Ce_{0.75}Zr_{0.25}O_2$ | 7 | 300 | 3.27 | 3.53 | 79.06 | 14.15 | 7.79 | 13.19 |
| $Au/CeO_2$ | 1 | 300 | 0.95 | - | 99.05 | - | 7.68 | < 5 |
| $Au/CeO_2$ | 1 | 400 | 0.86 | - | 99.14 | - | 8.29 | < 5 |
| $Ce_{0.75}Zr_{0.25}O_2$ support | - | 400 | - | - | 83.62 | 16.38 | 7.85 | - |
| $CeO_2$ support | - | 400 | - | - | 100.00 | - | 8.83 | - |
| Spent $Au/CeO_2$ PROX 1[c] | 1 | 400 | 0.83 | - | 99.17 | - | 8.50 | < 5 |
| Spent $Au/CeO_2$ PROX 2[c] | 1 | 400 | 0.85 | - | 99.15 | - | 8.23 | < 5 |

*measured from XRF.

[a]Mean crystallite sizes were calculated from the average values of $CeO_2$ plane (111), (200), (220), and (311).

[b]Au crystallite size was calculated from the diffraction plane (111).

[c]Spent catalyst from the realistic reformate after exposure to the stability testing.

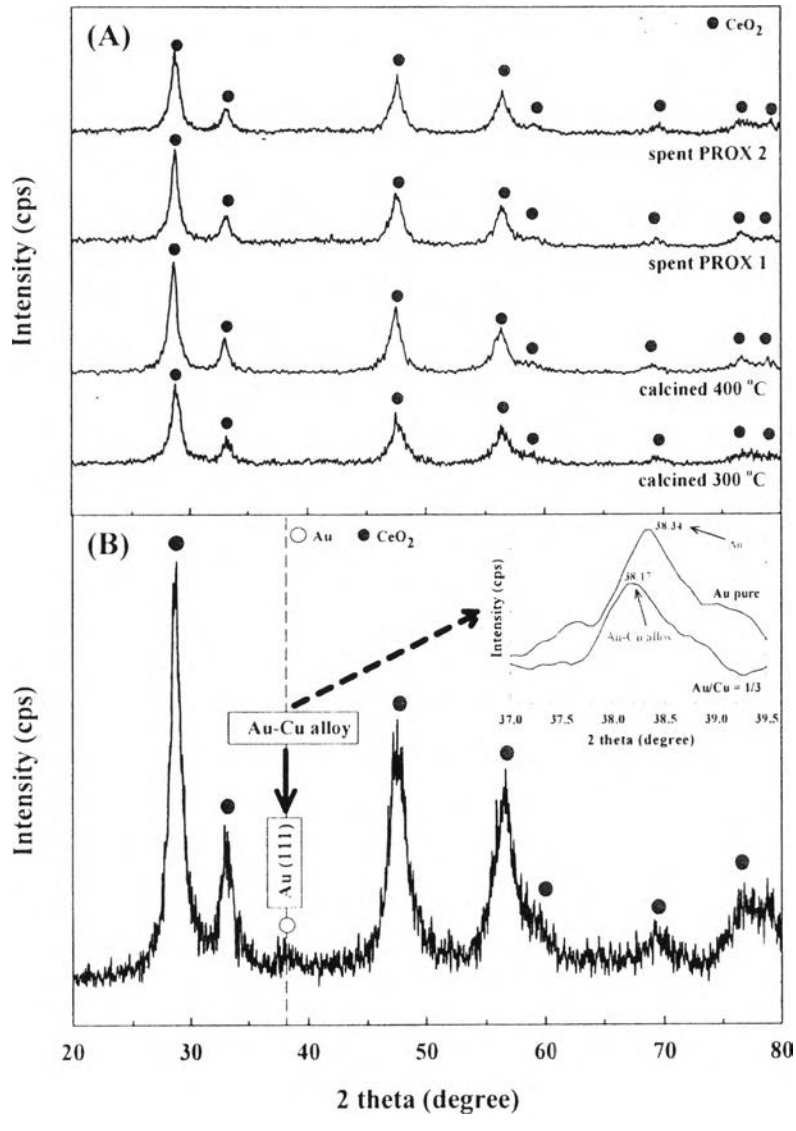


**Figure 8.2** XRD patterns of the (A) fresh and spent 1 wt% $Au/CeO_2$ catalysts, and (B) 7 wt% $Au–Cu/CeO_2–ZrO_2$ catalyst.

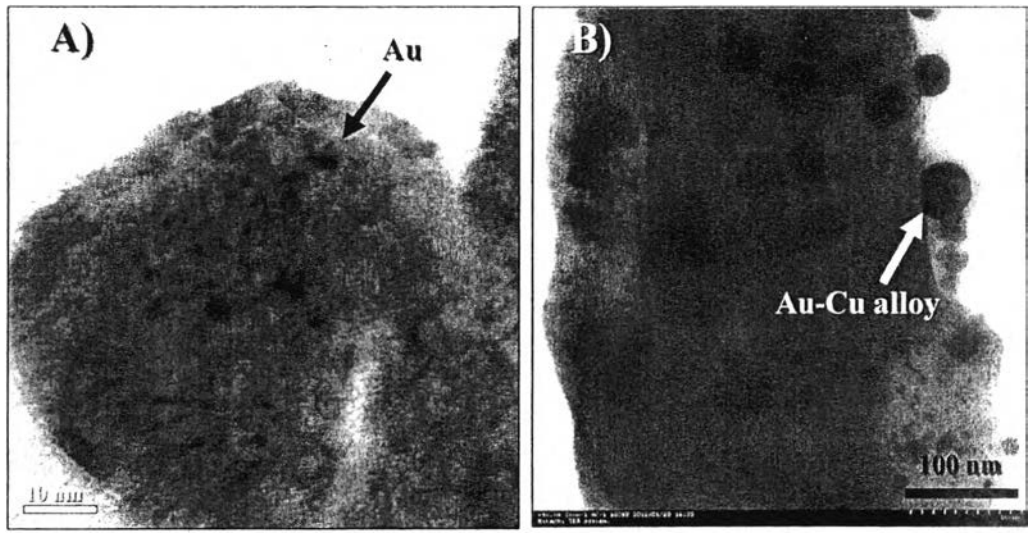


**Figure 8.3** TEM images of the (A) 1 wt% $Au/CeO_2$ calcined at 400 °C and (B) 7 wt% $Au–Cu/CeO_2–ZrO_2$ catalysts calcined at 300 °C.

According to the $H_2$-TPR profile, as shown in Fig. 8.4, it was used to analyze the difference in interaction site and number of $H_2$ consumption in different catalysts. The $CeO_2$ support presented the temperature peak at 487 °C being matched with the oxygen surface reduction, and the high temperature peak at 817 °C that was attributed to the $CeO_2 \rightarrow Ce_3O_4$ bulk reduction [4]. After depositing Au metal, these two support peaks slightly shifted toward lower temperatures at 468 °C and 809 °C, respectively, postulating that an active Au metal strongly interacted with the $CeO_2$ support to cause better reducibility [29,30]. The lowest reduction temperatures of 114–123 °C within very high intensities were assigned to the $Au_xO_y$ or cationic Au ($Au^{\delta+}$) reduction [4]. When increasing calcination temperature, the amount of $H_2$ consumption substantially decreased without any changes in support reduction. It was noteworthy that calcination was "thermal treatment" that was able to reduce the $Au^{\delta+}$ to Au metallic ($Au^0$) state, being less reductive [4,17]. Taking into account the area under the Au reduction peak relating with the amount of $H_2$ consumed on $Au^{\delta+}$ site, the more Au reduction area were, the more $H_2$ and $Au^{\delta+}$ number were used in the reduction process. With this knowledge, it was reasonable to conclude that the $Au/CeO_2$ calcined at 400 °C had more $Au^0$ (or less $Au^{\delta+}$) species than those of 300

°C. For the shifting of Au reduction toward lower temperature (123→114 °C), it could represent an easier and better reducibility of the Au sites on the catalyst surface and the strong Au–Au (metal–metal) interaction, which has been reported previously [4,5].

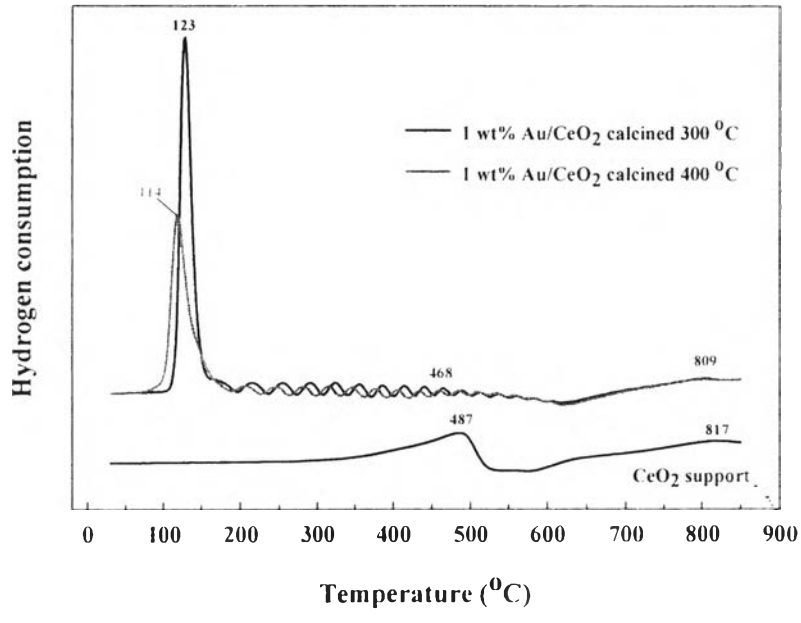


**Figure 8.4** TPR profiles of 1 wt% $Au/CeO_2$ catalysts calcined at 300 and 400 °C.

8.4.2 Single-stage PROX Performance

According to the Fig. 8.5, starting with using 100 mg of 1 wt% $Au/CeO_2$, it was clearly seen that the overall trends of CO conversion decreased with increasing reaction temperature for both $O_2$/CO ratios due to competitive $H_2$ oxidation at high temperature [16]. The lowest catalytic activity was found at the $O_2$/CO ratio of 0.5 in the whole studied temperature of 90–150 °C, where the CO conversion and $O_2$ conversion (not shown here) were in the range of ~5–37 % and ~10–27 %, respectively. Although the unity $O_2$/CO feed ratio slightly enhanced the CO conversion up to 9–45 % together with the significant improvement of $O_2$ conversion to 60–70 %, the amount of CO remaining at the output stream was still very high at 7000–12000 ppm. This initial study, at least, suggested that an insufficient $O_2$ feeding could not promote the efficient CO oxidation reaction [8];

moreover, we believed that there must be other factors that strongly affected the PROX activity such as calcination temperature and the amount of use catalyst. As expected, under the unity $O_2$/CO, the catalyst calcined at 400 °C gave ~25–49 % CO conversion (CO: 6800–9800 ppm) and ~69–74 % $O_2$ conversion, which were the consequences of the improvement of support crystallinity, stronger Au–Au interaction, and the combination of rich $Au^0$ and less $Au^{\delta+}$ species that were responsible for better PROX activity.

To better understand the role of $Au^{\delta+}/Au^0$ relative to PROX reaction, some researchers proposed that ionic $Au^{\delta+}$ specie was responsible for the low-temperature reaction, while the metallic $Au^0$ was active for steady-state high catalytic activity [31]. Sometimes, the co-existence of $Au^0$ and $Au^{\delta+}$ with appropriate amount was also active for the catalytic activity [21]. In this work, we interpreted that two types of Au species exhibited the combining positive effects for both low- and high-temperatures, and more $Au^0$ contents in the high calcined catalyst were also important for the activity in this experiment. However, the exactly active gold state is still unclear and has not yet been elucidated.

The use of different catalyst amount in the fixed bed reactor strongly influenced on the PROX performance [8,23], and the result revealed that CO conversion was maximized to ~59–65 %, resulting in the decrease in CO concentration from 13000 to 4550–5330 ppm after increasing the catalyst amount to 500 mg. The overall PROX activity was more stable at $T \geq 120$ °C after using higher amounts of catalyst due to the fact that the increasing in catalyst amount led to the increments of active $Au^0/Au^{\delta+}$ species, reactive surface areas, and longer contact time of the reactant gas. Hence, the PROX activity was then enhanced. Similarly, Sirichaiprasert et al. (2006) and Monyanon *et al.* (2006 and 2007) reported the increase in CO oxidation rate linking with the increasing of W/F (catalyst weight/volumetric feed flow rate) ratio [8,32,33]. When correlating with the space velocity, the increment in amount of catalyst used in the reactor led to the significant decrease in space velocity from 19800 to 3300 mL g-cat$^{-1}$ h$^{-1}$, where the efficient PROX performance was matched with the lower space velocity [34]. Interestingly, the PROX activity was dramatically suppressed to the lowest value when further

increasing the catalyst amount to 600 mg. The possible explanation was belonged to the retard of kinetic rate of PROX reaction by the high pressure drop inside the reactor tube after packing too much catalyst. Even though the use of 500 mg catalyst was the optimal condition, the main concerns were about the low conversions and the high CO-output concentration which was not acceptable to be applied in the PEMFC. To enhance the PROX performance, the use of double-stage PROX must be carried out under the same optimal condition as the single-stage one, and the $T_{1st\ stage}$ was fixed at 110 °C since this temperature was similar to that of PEMFC (80–120 °C).

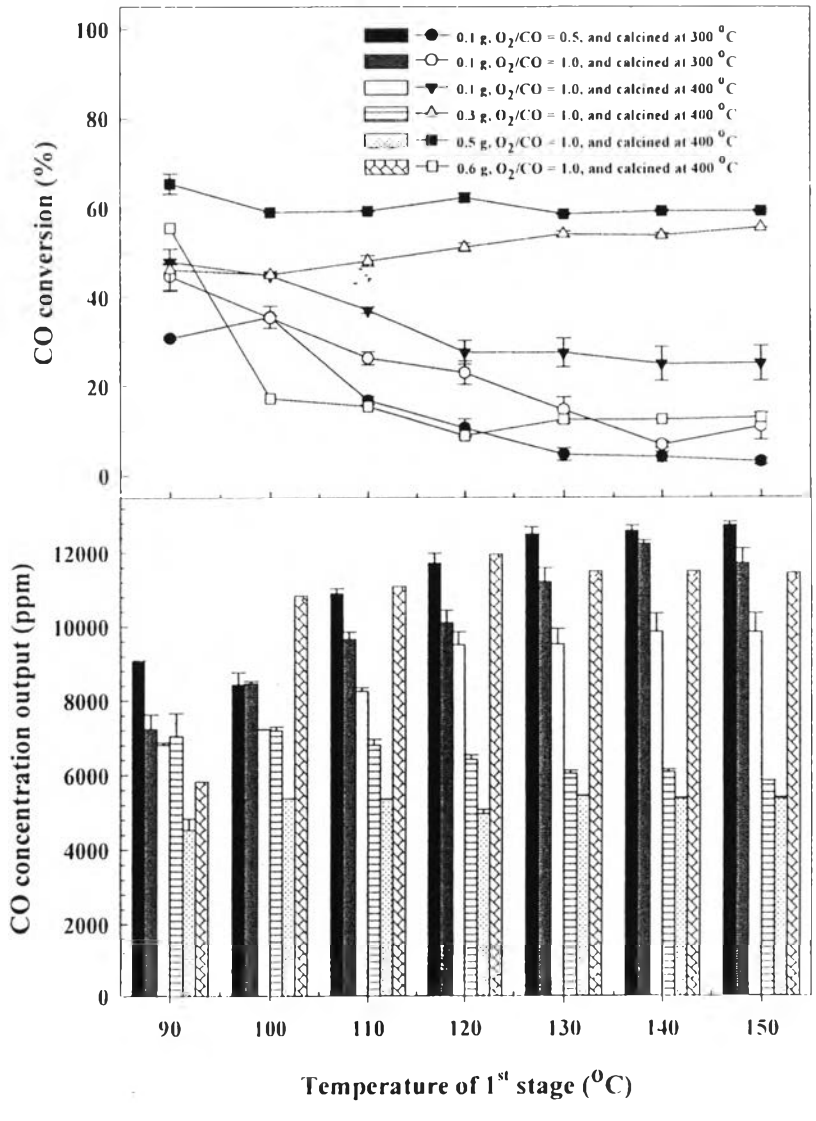


**Figure 8.5** Effects of $O_2$/CO molar ratio, calcination temperature, and amount of catalyst on the single-stage PROX activity under 1 wt% Au/$CeO_2$ catalyst.

### 8.4.3 Double-stage PROX Performance

#### *8.4.3.1 Effect of $O_2$ Split ratio*

It has been reported that the PROX performance was encouraged by introducing double-stage PROX [8,23]. Adjusting the amount of $O_2$ feeding in each reactor was expected to be one of the ways to efficiently remove CO. Under the same optimum conditions as single-stage (250 mg per each stage, $T_{1st\ stage}$ = 110 °C, and $O_2$/CO ratio = 1), the various $O_2$ split ratios ($1^{st}$ stage: $2^{nd}$ stage; 40:60, 50:50, and 60:40) were investigated as a function of $T_{2nd\ stage}$ of 90–150 °C, as shown in Fig 8.6. Even though the split of catalyst amount caused the decrease in W/F ratio in each stage to 0.008 g-cat*min $mL^{-1}$, the summation of each W/F value was still the same as that of single-stage reactor (0.016 g-cat*min $mL^{-1}$). It was apparently found that both CO and $O_2$ conversions were significantly enhanced in the window temperature. The maximum CO conversions were observed as following; 97–99 % at $T_{2nd\ stage} \leq 100$ °C for any ratios, and then decreased to the minimum values at 78–90 % after increasing $T_{2nd\ stage}$ to 150 °C. It seemed that the minimum conversion was much higher than that of single-stage PROX. For the $O_2$ conversion, the full $O_2$ conversion was obtained for the ratios of 50:50 and 60:40 in the whole range of $T_{2nd\ stage}$, wheareas that of 40:60 ratio decreased to ~65–79 % at $T_{2nd\ stage} \geq 110$ °C. However, these results confirmed that the addition of double-stage definitely improved the PROX performance in any $O_2$ split ratios, which were in agreement with many previous works [23,35,36].

When interpreting all results, the PROX activity in the $2^{nd}$ stage was divided into 2 sections; the low-temperature range (90–100 °C) and the high-temperature range (> 100 °C), in order to better understand the role of $O_2$ split ratio in the double-stage PROX. When focusing on the amount of $O_2$ fed into the $2^{nd}$ stage, it seemed that the increasing amount of $O_2$ in the $2^{nd}$ reactor (60:40→50:50) significantly enhanced the CO conversion at high-temperature range, while not affect much on the low-temperature conversion and full $O_2$ conversion. When applying the highest amount of $O_2$ in the $2^{nd}$ stage with 40:60 split ratio, the high-temperature CO conversion showed the slight drop of ~5 %, but the opposite result of high-temperature $O_2$ conversion was found with the significant drop to 65–79 %. These

results suggested that the increasing of $O_2$ amount in the 2nd stage reactor was necessary for the PROX improvement in the high-temperature range, while using too much $O_2$ feeding in the 2nd stage reactor gave the negative effect instead since this led to the lowest $O_2$ feeding amount into the 1st stage reactor, which might be not sufficient for the $O_2$ consumption and was probably responsible for the main $O_2$ consumption in this double-stage process. Hence, it was reasonable to conclude that the use of high $O_2$ amounts in both stage reactors was important to be balanced in order to achieve the high CO and $O_2$ conversions in both low- and high-temperature ranges. As mentioned previously, the $O_2$ split ratio of 50:50 was chosen as the optimum condition since it provided highly stable CO conversion at 90–95 % (CO-output concentration = 650–1300 ppm) and full $O_2$ conversion along the entire $T_{2nd\ stage}$.

*8.4.3.2 Effect of Weight Split ratio*

The use of catalyst amount in each stage was varied into 0.15:0.35, 0.25:0.25, and 0.35:0.15 under the total amount of 500 mg, as illustrated in Fig. 8.7. The weight split ratio substantially affected the CO conversion, while not impact the full $O_2$ conversion. The highest CO conversion of ~98 % was observed at $T_{2nd\ stage}$ of 90 °C for the 0.15:0.35 and 0.25:0.25 ratios, and 100 °C for the 0.15:0.35 ratio. For $T_{2nd\ stage}$ > 110 °C, the CO conversion decreased approximately 2–8 %, which was reasonable with the increase of CO concentration. The ratio of 0.15:0.35 obtained better CO conversion than that of 0.25:0.25, while the ratio of 0.35:0.15 gave the highest 95–97 % CO conversion (CO: 300–700 ppm) which tended to be the optimum condition. In fact, the overall trends of the PROX activity did not follow the trend of weight split ratio, probably due to the differences in rate of CO oxidation and W/F (or space velocity) in each stage. We suggested that the best catalytic activity did not always follow the use of high amounts of catalyst in both reactors, but it was matched with the suitable catalyst amount for each reactor to achieve the best performance.

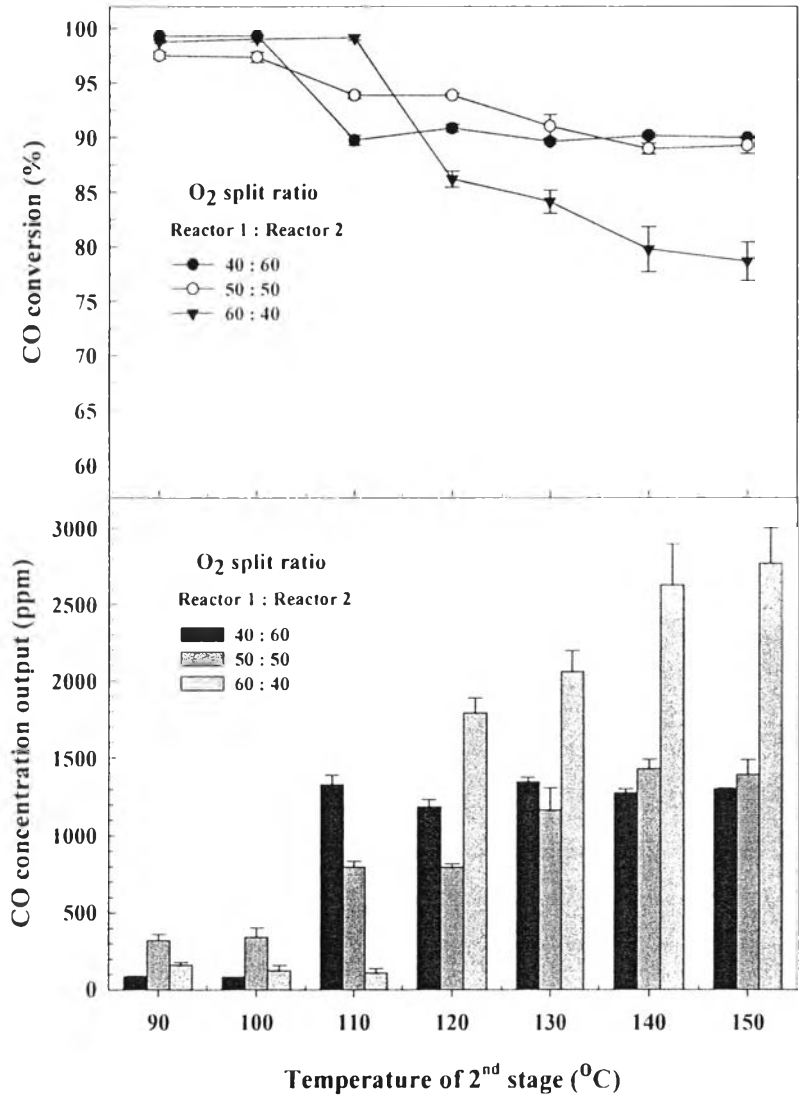


**Figure 8.6** Effect of $O_2$ split ratio on the double-stage PROX activity under 1 wt% $Au/CeO_2$ catalyst calcined at 400 °C. (Reaction conditions: $O_2/CO$, 1; weight split ratio, 0.25:0.25; $T_{1st\ stage}$, 110 °C.)

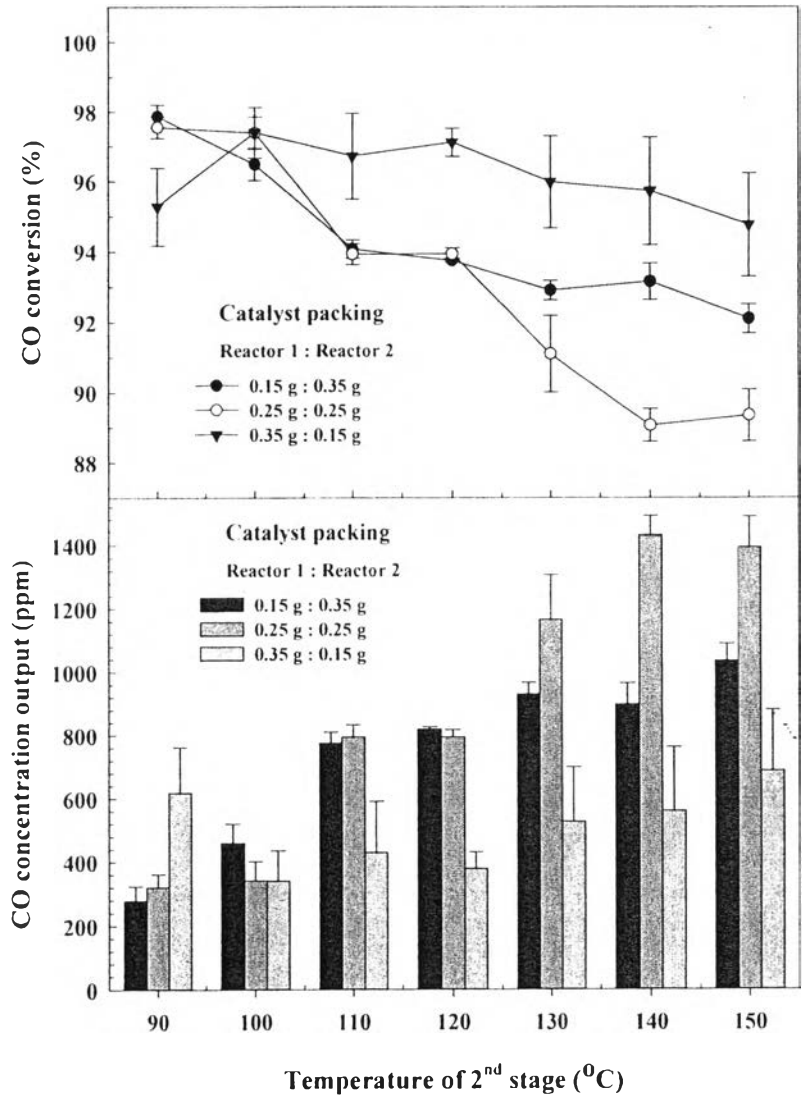


**Figure 8.7** Effect of the weight split ratio on the double-stage PROX activity under 1 wt% $Au/CeO_2$ catalyst calcined at 400 °C. (Reaction conditions: $O_2/CO$, 1; $O_2$ split ratio, 50:50; $T_{1st\ stage}$, 110 °C.)

*8.4.3.3 Effect of Reaction temperature*

The operating temperature of each stage was also the important parameter for the optimization. In this experiment, the $T_{1st\ stage}$ was kept at constant temperatures—90, 100, and 110 °C—with varying the $T_{2nd\ stage}$ from 90 °C to 150 °C (Fig. 8.8). It seemed that the CO conversion strongly depended on the variation of $T_{1st\ stage}$ during the whole range of $T_{2nd\ stage}$. The CO conversion dramatically decreased to 80–86 % and 67–72 % when decreasing the $T_{1st\ stage}$ to 100 °C and 90 °C, respectively. The full $O_2$ conversion was obtained for every $T_{2nd\ stage}$ with $T_{1st\ stage} \geq 100$ °C, whilst the lowest $T_{1st\ stage}$ initially provided ~80 % conversion, and then increased to 100 % at $T_{2nd\ stage}$ of 140 °C (not shown here). For the output CO concentration, the values increased to 1800–2600 ppm and 3700–4400 ppm at $T_{1st\ stage} < 110$ °C, respectively. These results revealed that the suppression in double-stage PROX performance was definitely occurred when decreasing $T_{1st\ stage}$ to be lower than the appropriate value of 110 °C. The possible explanations were that (i) the decrease in reaction temperature of the 1$^{st}$ stage could lower the rate of CO oxidation and the rate of $O_2$ consumption in terms of kinetic relation that resulted in the large suppression in overall CO and $O_2$ conversions of the process, and (ii) the lower $T_{1st\ stage}$ could cause the partial condensation of the steam, contaminating in the reformate, that was able to deactivate the catalyst surface as well. However, the optimal conditions was found at the uses of $T_{1st\ stage} = 110$ °C and $T_{2nd\ stage} = 100$ °C which minimized the output CO concentration to 300 ppm.

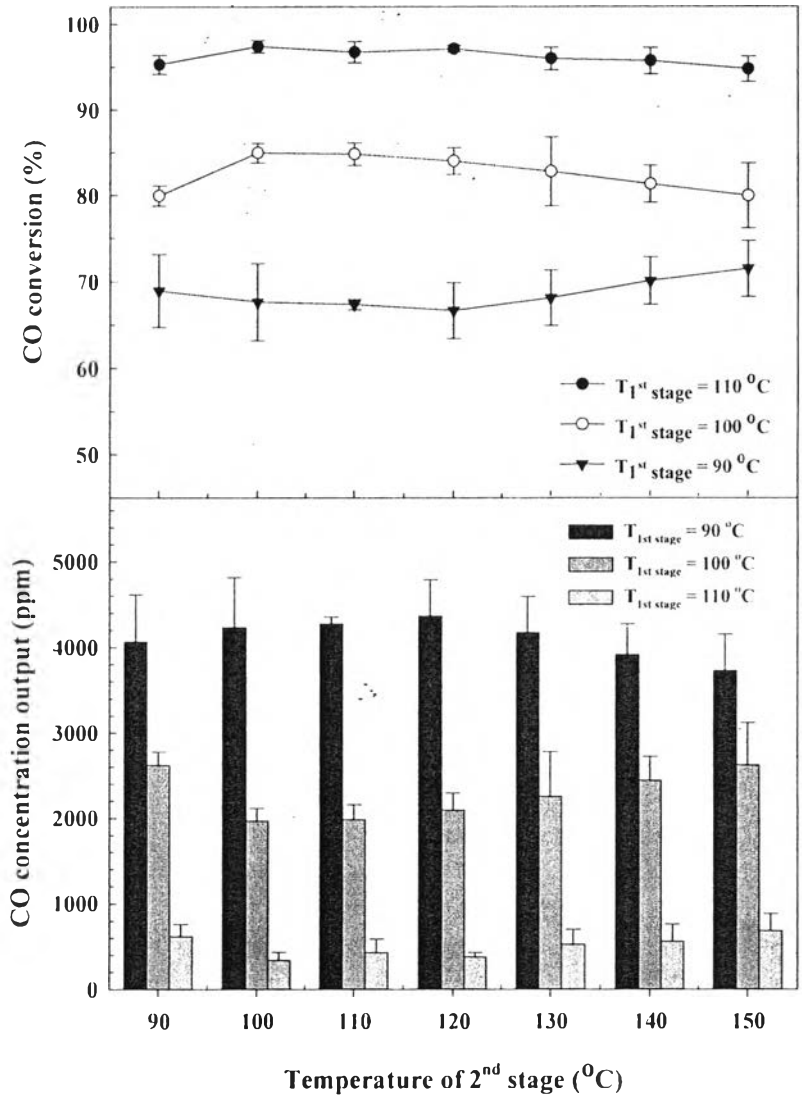


**Figure 8.8** Effect of the first-stage reaction temperature on the double-stage PROX activity under 1 wt% Au/$CeO_2$ catalyst calcined at 400 °C. (Reaction conditions: $O_2$/CO, 1; $O_2$ split ratio, 50:50; weight split ratio, 0.35:0.15.)

8.4.4 Stability Testing

From all studies, the best conditions—$O_2$ split ratio = 50:50, weight split ratio = 0.35:0.15, $T_{1st\ stage}$ = 110 °C, and $T_{2nd\ stage}$ = 100 °C—of the double-stage PROX were tested for the stability for 20 h in order to assess the capability of the MFP, and the result of the Fig. 8.9 showed the superior activity in which no deactivation in the full $O_2$ conversion during the time on stream, while there was

only slight drop in CO conversion from 97.8 % to 94 % after the first hour of experiment. The trend of CO concentration followed the trends of CO conversion, where it decreased significantly from 13000 ppm to 300 ppm at the initial time, and then increased to 800 ppm until the end of the experiment. The small reduction in activity was probably caused by the partial blockage of the catalyst active sites by the adsorbed water, intermediate carbonate species, or the CO–$H_2O$ surface complexes [34,37].

Taking into account the whole performance of MFP, we defined both $H_2$ purity (% mole) and CO concentration as the most two important measurements to identify the efficiency of this fuel processor. Eventhough there was no significant change in $H_2$ purity of the reformate (81–83 %) after passing the PROX unit, the overall process performance was still not good enough for using in the PEMFC directly since the CO concentration remaining from this process should be less than 10 ppm. Hence, the development and optimization in this process have to be further investigated on other parameters. Nonetheless, the beneficial ideas for using this MFP were, at least, reflected of (i) the high purity of $H_2$ gas, (ii) extreme reduction of CO concentration, and (iii) the use of low operating temperature of PROX (100–110 °C) that was almost the same as that in PEMFC, so there was no need of conducting heater or cooler utility before sending the product streams to the fuel cell.

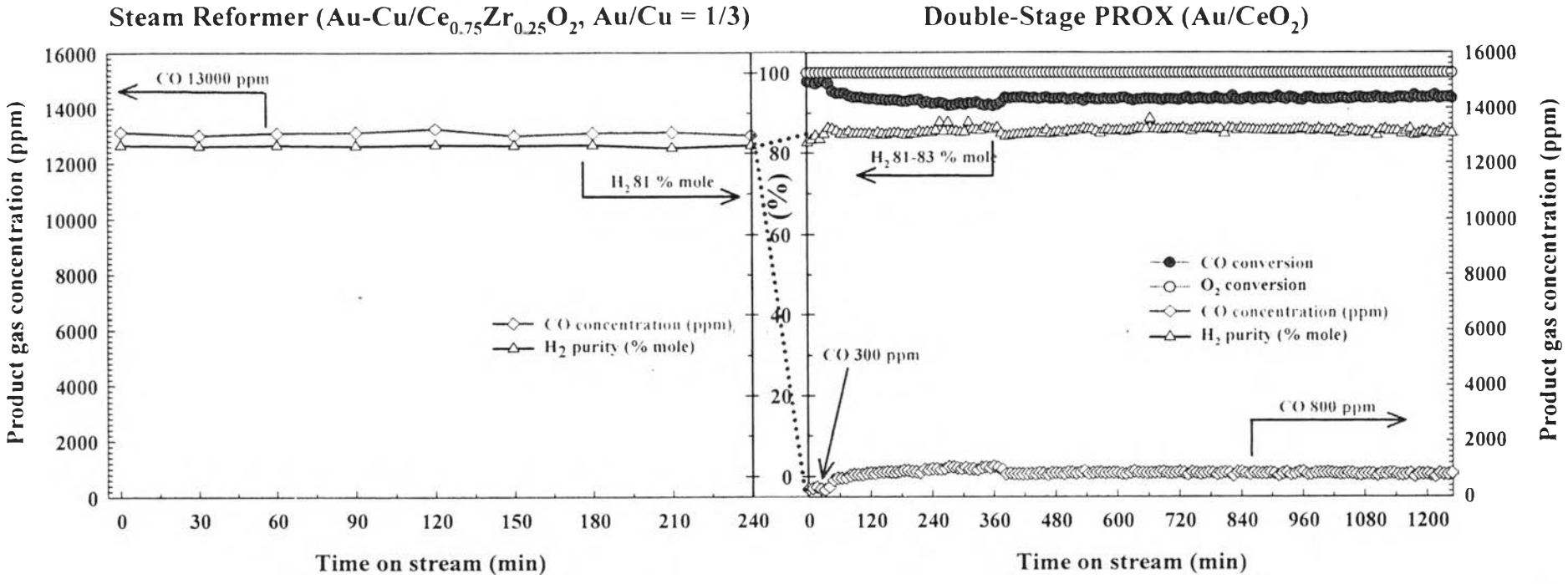


**Figure 8.9** Stability observation on the MFP process for 24 h. (Reaction conditions of double-stage PROX: $O_2$/CO, 1; $O_2$ split ratio, 50:50; weight split ratio, 0.35:0.15; $T_{1st\ stage}$, 110 °C; $T_{2nd\ stage}$, 100 °C.)

To confirm the appearances of these blocking adsorbed species, the FTIR characterization was used to detect some functional groups remaining on the surface of the spent catalysts of each stage, as shown in Fig. 8.10A and B. The spectra were separately detected into 2 ranges; (A) 2000–3800 $cm^{-1}$ and (B) 500–1800 $cm^{-1}$. Unlike the fresh catalyst, the strong band of 3200–3600 $cm^{-1}$, which matched with the hydroxyl (OH) group possibly coming from the unreacted steam of the steam reformer, became strongly pronounced in the spent catalysts. This postulated that the steam probably blocked the active sites of the surface of Au catalyst and kept staying until the end of experiment. In addition, there were the detectable bands of various carbonate ($-CO_3^{2-}$; 853, 1062, 1329 $cm^{-1}$) and bicarbonate ($-CO_3H$; 1522–1637 $cm^{-1}$) species on the fresh catalyst surface, which have been reported as the adsorbed species on the reduced ceria [4,38–40]. It inferred that these carbonate species were from the $Na_2CO_3$ that used in the catalyst preparing procedure. This kind of carbonate observation has been proposed in the fresh $Au/CeO_2$–$Fe_2O_3$ catalyst by using Temperature-program oxidation (TPO) characterization [5]. For the spent catalysts in each stage, the main carbonate bands at of 1200–1700 $cm^{-1}$ became strongly pronounced after exposure to the reaction, which might be generated from the complex mechanisms on the Au catalyst surface, such as the dehydration between bicarbonate and hydroxyl species or the adsorption of $CO_2$ product [38,41]. Meanwhile, the decrease in intensity of some small carbonate bands at 853–856 and 1060–1065 $cm^{-1}$ was found with the existence of the linear $CO_2$ adsorbed specie at 2348–2352 $cm^{-1}$. This postulated that the co-existence of steam might partially decompose carbonate [42,43] to form less stable bicarbonate, and then continually changed to $CO_2$ adsorbed species [44]. In some cases, the positive effect of the steam addition was found to promote the PROX and WGS catalysts [37,45,46]. However, the exact mechanisms were not discussed in this paper. From the XRD measurement of the spent catalysts in each stage, the presences of unchanged ceria crystallite size and diffraction planes evidenced that the structure of the catalyst did not change or collapse much during the reaction.

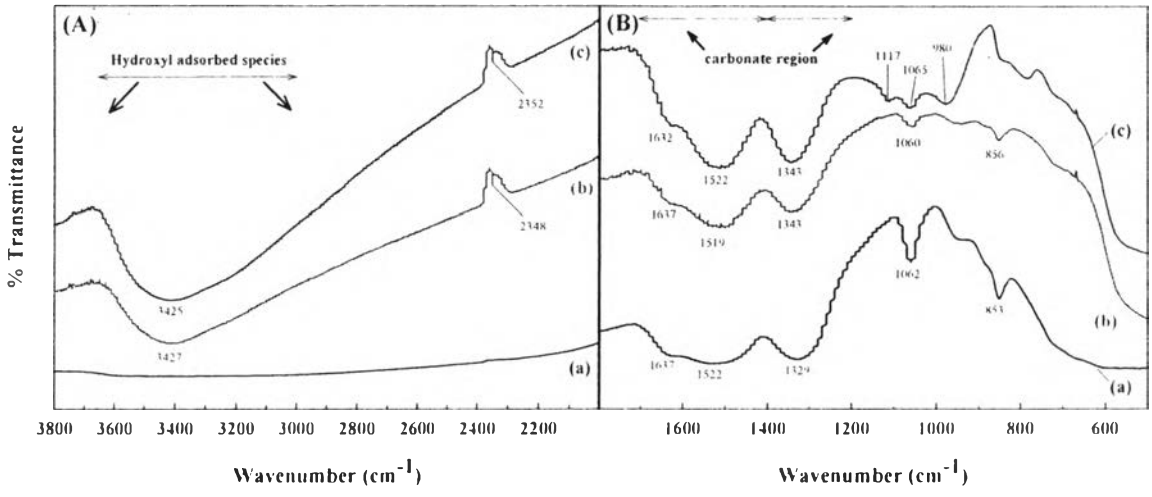


**Figure 8.10** FTIR analysis of 1 wt% $Au/CeO_2$ catalysts calcined at 400 °C: (A; 2000–3800 $cm^{-1}$, B; 700–1800 $cm^{-1}$) (a) Fresh catalyst. After exposure to the PROX reaction: (b) spent catalyst from the first stage and (c) spent catalyst from the second stage.

## 8.5 Conclusions

The development of MFP was successfully achieved by the use of 7 wt% $Au–Cu/Ce_{0.75}Zr_{0.25}O_2$ in the SRM unit and 1 wt% $Au/CeO_2$ in the PROX unit in order to produce the high $H_2$ purity with minimum CO contaminating content. The double-stage reactors showed much higher CO oxidation activity than that of single-stage reactor, where the CO concentration was reduced from 13000 ppm to 300–700 ppm in the temperature range of 90–150 °C. The optimum conditions were found in the $O_2$ split ratio of 50:50, weight split ratio of 0.35:0.15, and the first-stage temperature of 110 °C under the total amount of 500 mg use catalyst and the $O_2$/CO feed molar ratio of 1, which gave the highest CO conversion of 97.8 % and full $O_2$ conversion. Among of these effective parameters, the decreasing in the first-stage temperature presented severely negative effect than others. From the stability observation, the catalyst was suitable to be the long life-time catalyst without any degradation for 22 h. Since the CO concentration from the MFP was still at 300 ppm, the investigation of other parameters for double-stage PROX must be further carried

on to reduce the CO content lower than 10 ppm before continually applying in the PEM fuel cell.

## 8.6 Acknowledgements

The authors acknowledge the contributions and financial support of the following organizations: the Thailand Research Fund through the Royal Golden Jubilee Ph.D. Program (Grant No. PHD/0282/2552); the National Center of Excellence for Petroleum, Petrochemicals, and Advanced Materials, Chulalongkorn University; and The National Research University Project of CHE and the Ratchadaphiseksomphot Endowment Fund (EN276B).

## 8.7 References

[1] R. Tesser, M. Di Serio, E. Santacesaria, Methanol steam reforming: A comparison of different kinetics in the simulation of a packed bed reactor, Chem. Eng. J. 154 (2009) 69–75.

[2] K. Faungnawakij, R. Kikuchi, K. Eguchi, Thermodynamic evaluation of methanol steam reforming for hydrogen production, J. Power Sources 161 (2006) 87–94.

[3] V. Galvita, K. Sundmacher, Cyclic water gas shift reactor (CWGS) for carbon monoxide removal from hydrogen feed gas for PEM fuel cells, Chem. Eng. J. 134 (2007) 168–174.

[4] C. Pojanavaraphan, A. Luengnaruemitchai, E. Gulari, Hydrogen production by oxidative steam reforming of methanol over $Au/CeO_2$ catalysts, Chem. Eng. J. 192 (2012) 105–113.

[5] C. Pojanavaraphan, A. Luengnaruemitchai, E. Gulari, Effect of support composition and metal loading on Au catalyst activity in steam reforming of methanol, Int. J. Hydrogen Energy 37 (2012) 14072–14084.

[6] L. Bobrova, I. Zolotarsky, V. Sadykov, V. Sobyanin, Hydrogen-rich gas production from gasoline in a short contact time catalytic reactor, Int. J. Hydrogen Energy 32 (2007) 3698–3704.

[7] X. Zhou, M. Meng, Z. Sun, Q. Li , Z. Jiang, Prominent enhancement of Mn or Co addition on the performance of Cu-Ce-O catalyst used for $H_2$ production via dimethyl ether steam reforming, Chem. Eng. J. 174 (2011) 400–407.

[8] K. Sirichaiprasert, S. Pongstabodee, A. Luengnaruemitchai, Single- and double-stage catalytic preferential CO oxidation in $H_2$-rich stream over an $\alpha$-$Fe_2O_3$-promoted CuO–$CeO_2$ catalyst, J. Chin. Inst. Chem. Eng. 39 (2008) 597–607.

[9] L. Salemme, L. Menna, M. Simeone, Thermodynamic analysis of ethanol processors –PEM fuel cell systems, Int. J. Hydrogen Energy 35 (2010) 3480–3489.

[10] D. Montané, E. Bolshak, S. Abelló, Thermodynamic analysis of fuel processors based on catalytic-wall reactors and membrane systems for ethanol steam reforming, Chem. Eng. J. 175 (2011) 519–533.

[11] M.S. Wilson, Methanol decomposition fuel processor for portable power applications, Int. J. Hydrogen Energy 34 (2009) 2955–2964.

[12] J.M. Sohn, Y.C. Byun, J.Y. Cho, J. Choe, K.H. Song, Development of the integrated methanol fuel processor using micro-channel patterned devices and its performance for steam reforming of methanol, Int. J. Hydrogen Energy 32 (2007) 5103–5108.

[13] S. Monyanon, A. Luengnaruemitchai, S. Pongstabodee, Optimization of methanol steam reforming over a Au/CuO–$CeO_2$ catalyst by statistically designed experiments, Fuel Process. Technol. 96 (2012) 160–168.

[14] M. Schuessler, M. Portscher, U. Limbeck, Monolithic integrated fuel processor for the conversion of liquid methanol, Catal. Today 79–80 (2003) 511–520.

[15] Y. Men, G. Kolb, R. Zapf, D. Tiemann, M. Wichert, V. Hessel, H. Löwe, A complete miniaturized microstructured methanol fuel processor/fuel cell system for low power applications, Int. J. Hydrogen Energy 33 (2008) 1374–1382.

[16] P. Naknam, A. Luengnaruemitchai, S. Wongkasemjit, Preferential CO oxidation over Au/ZnO and Au/ZnO–$Fe_2O_3$ catalysts prepared by photodeposition, Int. J. Hydrogen Energy 34 (2009) 9838–9846.

[17] G.C. Bond, C. Louis, D.T. Thompson, Catalysis by Gold, volume 6, Imperial College Press, London, 2006.

[18] T.C. Ou, F.W. Chang, L.S. Roselin, Production of hydrogen via partial oxidation of methanol over bimetallic Au–Cu/$TiO_2$ catalysts, J. Mol. Catal. A: Chem. 293 (2008) 8–16.

[19] F.W. Chang, T.C. Ou, L.S. Roselin, W.S. Chen, S.C. Lai, H.M. Wu, Production of hydrogen by partial oxidation of methanol over bimetallic Au–Cu/$TiO_2$–$Fe_2O_3$ catalysts, J. Mol. Catal. A: Chem. 313 (2009) 55–64.

[20] C. Pojanavaraphan, A. Luengnaruemitchai, E. Gulari, Catalytic activity of Au–Cu/$CeO_2$–$ZrO_2$ catalysts in steam reforming of methanol, Appl. Catal. A: Gen. 456 (2013) 135–143.

[21] C. Pojanavaraphan, A. Luengnaruemitchai, E. Gulari, Effect of catalyst preparation on Au/$Ce_{1-x}Zr_xO_2$ and Au–Cu/$Ce_{1-x}Zr_xO_2$ for steam reforming of methanol, Int. J. Hydrogen Energy 38 (2013) 1348–1362.

[22] S. Scirè, C. Crisafulli, P.M. Riccobene, G. Patanè, A. Pistone, Selective oxidation of CO in $H_2$-rich stream over Au/$CeO_2$ and Cu/$CeO_2$ catalysts: An insight on the effect of preparation method and catalyst pretreatment, Appl. Catal. A: Gen. 417–418 (2012) 66–75.

[23] A. Luengnaruemitchai, P. Naknam, S. Wongkasemjit, Investigation of Double-Stage Preferential CO Oxidation Reactor over Bimetallic Au–Pt Supported on A-Zeolite Catalyst, Ind. Eng. Chem. Res. 47 (2008) 8160–8165.

[24] J. Kunming, Z. Huili, L. Wencui, Effect of morphology of the ceria support on the activity of Au/$CeO_2$ catalysts for CO oxidation, Chin. J. Catal. 29 (2008) 1089–1092.

[25] C.H. Kim, L.T. Thompson, Deactivation of Au/$CeO_x$ water gas shift catalysts, J. Catal. 230 (2005) 66–74.

[26] F. Zhang, C.H. Chen, J.C. Hanson, R.D. Robinson, I.P. Herman, S.W. Chan, Phases in Ceria-Zirconia Binary Oxide (1-x)$CeO_2$–x$ZrO_2$ Nanoparticles: The Effect of Particle Size, J. Am. Ceram. Soc. 89 (2006) 1028–1036.

[27] X. Liu, A. Wang, L. Li, T. Zhang, C.Y. Mou, J.F. Lee, Structural changes of Au–Cu bimetallic catalysts in CO oxidation: In situ XRD, EPR, XANES, and FT-IR characterizations, J. Catal. 278 (2011) 288–296.

[28] J. Llorca, M. Domínguez, C. Ledesma, R.J. Chimentão, F. Medina, J. Sueiras, I. Angurell, M. Seco, O. Rossell, Propene epoxidation over $TiO_2$-supported

Au–Cu alloy catalysts prepared from thiol-capped nanoparticles, J. Catal. 258 (2008) 187–198.

[29] G. Jacobs, U.M. Graham, E. Chenu, P.M. Patterson, A. Dozier, B.H. Davis, Low-temperature water–gas shift: impact of Pt promoter loading on the partial reduction of ceria and consequences for catalyst design, J. Catal. 299 (2005) 499–512.

[30] B. Campo, C. Petit, M.A. Volpe, Hydrogenation of crotonaldehyde on different $Au/CeO_2$ catalysts, J. Catal. 254 (2008) 71–78.

[31] L. Chang, N. Sasirekha, B. Rajesh, Y. Chen, CO oxidation on ceria- and manganese oxide-supported gold catalysts, Sep. Purif. Technol. 58 (2007) 211–218.

[32] S. Monyanon, S. Pongstabodee, A. Luengnaruemitchai, Preferential oxidation of carbon monoxide over Pt, Au monometallic catalyst, and Pt–Au bimetallic catalyst supported on ceria in hydrogen-rich reformate, J. Chin. Inst. Chem. Eng. 38 (2007) 435–441.

[33] S. Monyanon, S. Pongstabodee, A. Luengnaruemitchai, Catalytic activity of $Pt–Au/CeO_2$ catalyst for the preferential oxidation of CO in $H_2$-rich stream, J. Power Sources 163 (2006) 547–554.

[34] A. Luengnaruemitchai, M. Nimsuk, P. Naknam, S. Wongkasemjit, S. Osuwan, A comparative study of synthesized and commercial A-type zeolite-supported Pt catalysts for selective CO oxidation in $H_2$-rich stream, Int. J. Hydrogen Energy 33 (2008) 206–213.

[35] H. Igarashi, H. Uchida, M. Suzuki, Y. Sasaki, M. Watanabe, Removal of carbon monoxide from hydrogen-rich fuels by selective oxidation over platinum catalyst supported on zeolite, Appl. Catal. A: Gen. 159 (1997) 159–169.

[36] S. Srinivas, E. Gulari, Preferential CO oxidation in a two-stage packed-bed reactor: Optimization of oxygen split ratio and evaluation of system robustness, Catal. Commun. 7 (2006) 819–826.

[37] P. Naknam, A. Luengnaruemitchai, S. Wongkasemjit, Preferential CO oxidation over Au/ZnO and $Au/ZnO–Fe_2O_3$ catalysts prepared by photodeposition, Int. J. Hydrogen Energy 34 (2009) 9838–9846.

[38] T. Tabakova, F. Boccuzzi, M. Manzoli, D. Andreeva, FTIR study of low-temperature water-gas shift reaction on gold/ceria catalyst, Appl.Catal. A: Gen. 252 (2003) 385–397.

[39] S. Hilaire, X. Wang, T. Luo, R.J. Gorte, J. Wagner, A comparative study of water-gas-shift reaction over ceria-supported metallic catalysts, Appl. Catal. A: Gen. 258 (2004) 271–276.

[40] C. Pojanavaraphan, A. Luengnaruemitchai, E. Gulari, Effect of steam content and $O_2$ pretreatment on the catalytic activities of $Au/CeO_2$–$Fe_2O_3$ catalysts for steam reforming of methanol, J. Ind. Eng. Chem. 20 (2014) 961–971.

[41] C. Binet, M. Daturi, J.C. Lavalley, IR study of polycrystalline ceria properties in oxidised and reduced states, Catal. Today 50 (1999) 207–225.

[42] C.K. Costello, J.H. Yang, H.Y. Law, Y. Wang, J.N. Lin, L.D. Marks, M.C. Kung, H.H. Kung, On the potential role of hydroxyl groups in CO oxidation over $Au/Al_2O_3$, Appl. Catal., A 243 (2003) 15–24.

[43] A. El-Moemen, A. Karpenko, Y. Denkwitz, R.J. Behm, Activity, stability and deactivation behavior of $Au/CeO_2$ catalysts in the water gas shift reaction at increased reaction temperature (300 °C), J. Power Sources 190 (2009) 64–75.

[44] A. Karpenko, R. Leppelt, J. Cai, V. Plzak, A. Chuvilin, U. Kaiser, R.J. Behm, Deactivation of a $Au/CeO_2$ catalyst during the low-temperature water–gas shift reaction and its reactivation: A combined TEM, XRD, XPS, DRIFTS, and activity study, J. Catal. 250 (2007) 139–150.

[45] D. Andreeva, T. Tabakova, V. Idakiev, P. Christov, R. Giovanoli, $Au/\alpha$-$Fe_2O_3$ catalyst for water-gas shift reaction prepared by deposition–precipitation, Appl. Catal., A 169 (1998) 9–14.

[46] P. Naknam, A. Luengnaruemitchai, S. Wongkasemjit, S. Osuwan, Preferential catalytic oxidation of carbon monoxide in presence of hydrogen over bimetallic AuPt supported on zeolite catalysts, J. Power Sources 165 (2007) 353–358.